

# Potential impacts of the spring-neap tidal cycle on shelf sea primary production.

Jonathan Sharples  
Proudman Oceanographic Laboratory  
6 Brownlow Street  
Liverpool L3 5DA  
United Kingdom

j.sharples@pol.ac.uk  
tel: +44 151 795 4800  
fax: +44 151 795 4801

Keywords: tidal mixing, spring-neap cycle, shelf seas, fronts, phytoplankton, primary production, carbon fluxes

Running header: *The spring-neap cycle and primary production*

Submitted to *Journal of Plankton Research*, July 5<sup>th</sup> 2007

Resubmitted to *Journal of Plankton Research*, September 28<sup>th</sup> 2007

Accepted by *Journal of Plankton Research*: October 22<sup>nd</sup> 2007

## Abstract

Spring-neap modulation of tidal mixing could potentially have significant effects on the timing and magnitude of primary production in stratified shelf seas. A 1-dimensional turbulence model, coupled to a simple model of primary production, is used to identify potential spring-neap impacts. Changes in the timing of the spring-neap cycle could contribute 10% of inter-annual variability of bloom timing in weak tidal regimes and 25% in areas with stronger tidal currents. In stratified regions away from the tidal mixing fronts the spring-neap cycle is predicted to result in periodicity in the biological rates within the thermocline, and the turbulent flux of organic carbon into the bottom water. The strongest impacts are predicted within 15 – 50 km of the tidal mixing fronts, with increases in sub-surface primary production and carbon export. At the fronts there is substantial extra primary production driven by the spring-neap cycle, contributing an extra 70% annually compared to fronts forced by the  $M_2$  tide only. This impact is reflected in the organic carbon mixed downward into the bottom waters near the front. The results have important implications for the interpretation of observations of primary production, and for the resolution required by shelf-wide models of the marine ecosystem.

## Introduction

Mixing by the barotropic tide exerts well-known controls on the physics and biochemistry of shelf seas. Away from coastal regions influenced by freshwater sources, the vertical physical structure of the water column is driven primarily by the competing effects of vertical mixing, predominantly tidally-driven in NW European shelf seas, and seasonally-varying solar heating (Simpson and Bowers, 1984). Deep regions, and/or regions with low tidal currents (such as the northern North Sea, the western English Channel, and the Celtic Sea) thermally stratify in spring and summer as the influence of solar irradiance overcomes the capacity for the tidal mixing to maintain a vertically homogeneous water column. Shallower areas or areas with strong tidal currents (e.g. the Irish Sea, southern North Sea, and the central English Channel) remain vertically-mixed all year as the strength of the tidal turbulence is always able to overcome the stratifying effect of the solar heating. The mixing and stratifying influences balance at the shelf sea tidal mixing fronts, the position of which can be described by the ratio of the total water depth to the cube of a measure of the tidal current strength (e.g. Simpson and Hunter, 1974; Simpson, 1981). The success of this approach in correctly predicting the frontal positions underlines the dominance of vertical exchange processes and the weak impacts of advection in these shelf seas, allowing many questions to be addressed in a 1-dimensional (vertical) framework.

This physical partitioning into seasonally-stratified, permanently-mixed, and frontal regimes is pivotal in determining the environment for primary production (Sharples and Holligan, 2006). In stratifying regions the development of a thermocline in spring alleviates the light-limited conditions experienced by the phytoplankton, leading to the rapid growth of the spring bloom in the new surface layer, followed by maintenance of new primary production within the thermocline during the summer (e.g. Pingree et al., 1976). The spring bloom is a critical event, being the first significant supply of organic fuel to the rest of the marine ecosystem following the winter. The timing of the bloom is known to play an important role for the growth and survival of other components of the marine ecosystem, e.g. copepods (Head et al., 2000), fish larvae (Platt et al., 2003), and seabirds (Frederiksen et al., 2006). Sub-surface growth of phytoplankton during the summer, while having typically lower biomass concentrations than the spring bloom, often has high f-ratios (Probyn et al., 1995) and is an important source of organic carbon to the ecosystem, thought to be comparable to the spring bloom in terms of its contribution to the total annual primary production in stratifying shelf seas (Richardson et al., 2000; Weston et al., 2005). Shelf sea fronts have long been associated with enhanced levels of phytoplankton biomass (Pingree et al., 1975; Tett et al., 1993) resulting from locally increased primary production (Horne et al., 1996; Maguer et al., 2000). Primary productivity at these fronts is also associated, probably causally, with increased densities of zooplankton, fish larvae, and foraging predators (e.g. Durazo et al., 1998; Sims and Quayle, 1998; Russell et al., 1999; Lough and Manning, 2001).

Against the background of the seasonality of meteorological forcing competing with some average measure of tidal mixing, investigations into the impacts of variability in mixing inputs on shelf sea primary production have primarily concentrated on the effects of variable wind stress. Variability in winds during spring is an important source of inter-annual variability in the timing of the spring bloom in shelf seas (Eslinger and Iverson, 2001; Sharples et al., 2006) and in the open ocean (Waniek, 2003), with impacts on the rest of the marine ecosystem. During the summer

stratified period short-term wind events are important in determining the physical structure of the surface layer and thermocline (Ridderinkhof, 1992), with episodic pulses of wind deepening the thermocline and either fuelling primary production in the sub-surface biomass maximum (Sharples and Tett, 1994) or entraining nutrients into the surface layer (Yin et al., 1995). Incorporating sufficient knowledge of surface wind variability is vital for correct simulations of ecosystem structure and annual primary production rates (Ruudij et al., 1997).

Other than the horizontal variations in mean tidal mixing that underlie the broad partitioning of shelf seas, very little emphasis has been placed on the impacts of tidally-driven variability on shelf sea primary production. In NW European shelf seas spring tidal currents are typically twice those during neap tides, implying a difference of a factor of 8 in the available mixing energy. Spring-neap tidal variability has been shown to play a role in the timing of the spring bloom, possibly by briefly interrupting the development of spring stratification (Sharples et al., 2006). Phytoplankton growth and ecosystem responses to the spring-neap cycle have been predicted with numerical models of the seasonal thermocline (Sharples, 1999; Allen et al., 2004) as a result of periodic erosion of the base of the summer thermocline by an approaching spring tide, followed by deepening stratification approaching the next neap tide. Direct observations of phytoplankton carbon flux from the thermocline into the bottom mixed layer have been suggested to be driven by the spring-neap mixing cycle (Sharples et al., 2001). There is a well-understood spring-neap adjustment in the position of shelf sea fronts (Simpson and Bowers, 1979) which is thought to provide a mechanism for supplying nutrients to frontal phytoplankton (Loder and Platt, 1985; Rogachev et al., 2001). There may be spring-neap contrasts in the generation of internal waves and the associated vertical fluxes of nitrogen to the photic zone at the shelf edge (Holligan et al., 1985; Sharples et al., 2007), while in coastal waters there is data to suggest that red tides tend to occur during the stronger stratification at neap tides (Balch, 1986).

This paper uses a numerical model to provide a first assessment of the broader implications of the spring-neap tidal cycle for annual production rates and vertical carbon fluxes in shelf seas, quantifying the potential contribution that the spring-neap tidal cycle may make to inter-annual variability in spring bloom timing and to primary production and carbon fluxes in the vicinity of shelf sea fronts.

## **Method**

Identifying spring-neap impacts on shelf sea primary production is inherently difficult observationally. While technically feasible, sufficiently long time series of vertical profiles of chlorophyll do not yet exist simply because of the cost of the required instrumentation. Time series of profiles of biological rates and vertical turbulent fluxes of nutrients are even more problematic, as existing methods rely on intensive ship-based experiments. Instead oceanographers are reliant on numerical models to fill in the gaps between often patchy observations, and to provide the observations with a broader context.

The approach here is to use a 1-dimensional (vertical) coupled physics-primary production numerical model to simulate annual cycles of stratification and phytoplankton growth for a typical NW European shelf sea, and to use the model output to construct vertical-horizontal slices of physical and biological properties

across a shelf sea tidal mixing front. The cross-frontal simulations follow an established method of synthesising a vertical slice through a shelf sea front by combining a series of 1-dimensional vertical profiles generated with different tidal current speeds and/or water column depth (Simpson and Sharples, 1994).

The physical model is identical to that used by Sharples et al., 2006, simulating the annual cycle of vertical temperature profiles in response to tidal mixing and seasonally-varying meteorology. The link between the efficiency of vertical turbulent mixing and the inhibiting effect of stratification is provided by a  $k - \varepsilon$  turbulence closure scheme (Canuto et al., 2001), with modified constants as described by Holt and Umlauf (in press). This closure scheme has been shown to be equivalent to the often-used Mellor-Yamada scheme (Burchard et al., 1998). Collecting the necessary observations in shelf seas suitable for verification of model turbulent parameters is in practice still very difficult. The schemes compare well with observations of boundary-driven turbulent dissipation in stratifying and mixed shelf seas (Simpson et al., 1996). Methodological limitations have so far prevented comparison with observations of turbulent kinetic energy, but the models have been well verified in laboratory flows (e.g. Patel et al., 1985). The applicability of these turbulence schemes for shelf sea modelling is underlined by the correct simulation of the timing of spring stratification and the inter-annual drift in the climate of the North Sea (Sharples et al., 2006), and the positions of the shelf sea tidal mixing fronts using both 1-D (Simpson and Sharples, 1994) and fully 3-D (Holt and Umlauf, in press) approaches.

The physical model is forced by smoothly-varying seasonal meteorology, and tidal conditions similar to the Celtic Sea. Seasonally-varying surface noon irradiance ( $I_{noon}$ ,  $W m^{-2}$ ) is calculated as the noon clear-sky irradiance for latitude  $50^\circ$ , modified by a smoothly varying (sinusoidal) cloudiness ranging from a winter value of 80% at the start and end of the year and a summer value of 50% in the middle of the year:

$$I_{noon} = 369 - 247 \cos(\omega_a t_{JD}) + 29 \sin(\omega_a t_{JD}) \quad (1)$$

with  $\omega_a = 0.017 d^{-1}$  the annual frequency and  $t_{JD}$  the time (days) expressed as the Julian Day ( $t_{JD} = 1$  day on January 1<sup>st</sup>). Surface irradiance has a diurnal cycle, using a sinusoidal variation with amplitude  $I_{noon}$  and the length of daylight varying seasonally for latitude  $50^\circ$ . Seasonally-varying daily means of wind speed ( $w$ ,  $m s^{-1}$ ), air temperature ( $T_{air}$ ,  $^\circ C$ ), air pressure ( $P_{air}$ , mbar), and relative humidity ( $RH$ , %) are provided by sinusoidal functions fitted to ERA-40 re-analysis of the output from the European Centre for Medium Range Weather Forecasting (ECMWF) numerical model for a position in the middle of the Celtic Sea in the year 1999:

$$T_{air} = 12.05 - 3.39 \cos(\omega_a t_{JD}) - 2.39 \sin(\omega_a t_{JD}) \quad (2)$$

$$w = \left( 65.5 + 31.5 \cos(\omega_a t_{JD}) + 2.5 \sin(\omega_a t_{JD}) \right)^{\frac{1}{2}} \quad (3)$$

$$P_{air} = (1.0140 - 0.0004 \cos(\omega_a t_{JD}) + 0.0009 \sin(\omega_a t_{JD})) \times 1000 \quad (4)$$

$$RH = 83.4 - 1.9 \cos(\omega_a t_{JD}) - 0.03 \sin(\omega_a t_{JD}) \quad (5)$$

Note that equation (3) is based on a fit to the square of the ERA-40 wind speed, to better describe the annual cycle of wind stress. The seasonality of the air-sea heat flux in a temperate shelf sea is primarily driven by the changing surface irradiance (Eqn. (1)) and the gradient between the sea surface temperature and the air temperature (Fig. 1A). There is some seasonality in the surface winds (Fig. 1B) captured by the fit to the seasonal function. A large amount of short-term wind variability is smoothed out by equation (3); while this variability is normally an important component of accurate simulations of shelf sea primary production, not including it here allows clear identification of spring-neap driven variability. Variability in relative humidity (Fig. 1C) and air pressure (Fig. 1D) is almost entirely associated with short-term weather events with very little seasonal signal. This dominance of surface irradiance and air temperature is consistent with analysis of observed positions of shelf sea fronts, with wind variability found to play a secondary role (e.g. Simpson, 1981). Smoothing out the meteorological events does remove an important source of environmental variability that is key to the maintenance of sub-surface phytoplankton growth in the thermocline in summer, primarily by episodic pulses of nutrients mixed upward from the bottom mixed layer (Sharples and Tett, 1994). To account for this variability a background turbulent diffusivity of  $1 \times 10^{-5} \text{ m}^2 \text{ s}^{-1}$  is included here, previously shown by Sharples and Tett, 1994, to represent adequately the mean effect of wind events in driving mixing at the thermocline.

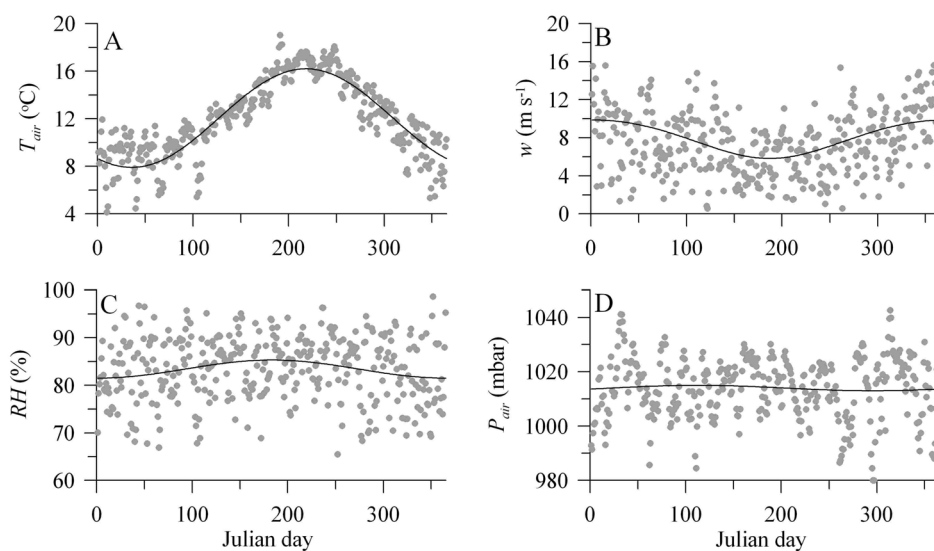


**Figure 1.**

Time series of the daily-mean meteorological data, (A) air temperature, (B) wind speed, (C) relative humidity, and (D) air pressure. The dots are data from the ERA-40 re-analysis, for a position in the central Celtic Sea and the year 1999. The lines are fits to a seasonal sinusoidal function (see equations (2) – (5)), showing most of the seasonality in the air temperature and wind speed, and smoothing out any short term weather influences.

In order to address the question of how spring-neap variations in tidal mixing might impact primary production the essential requirement is for a modelled primary producer that responds on realistic timescales to changes in the light and nutrient environment. A relatively simple model is used here, similar to that of Sharples and Tett, 1994. The biological model calculates the development of a single group of phytoplankton in response to light and dissolved inorganic nitrate, with the nitrate response incorporated using a cell-quota approach (Droop, 1974). Phytoplankton are

modelled in terms of carbon,  $P_C$  (mg m<sup>-3</sup>), and internal cellular nitrogen,  $P_N$  (mmol m<sup>-3</sup>), with the cell nitrogen quota  $Q = P_N/P_C$  (mmol N (mg C)<sup>-1</sup>). These biological state variables are treated in an Eulerian frame, diffusing vertically in response to the modelled turbulent diffusivity. Clearly it is an approximation; real phytoplankton cells and their constituents follow Lagrangian paths under the influence of turbulence, and ideally a Lagrangian model (e.g. Ross and Sharples, 2004) would be used. However, the computational demands of a Lagrangian approach make many problems, including the problem addressed by this paper, impractical. The Eulerian approximation is computationally much faster, and has been shown to result in prediction of primary production rates negligibly different (errors <3%) from the Lagrangian method (McGillicuddy, 1995). The disadvantage of the Eulerian approach is that some phenomena (e.g. physiologically-determined phytoplankton motility, Ross & Sharples, 2007) cannot be addressed; in this paper the results are restricted to those aspects of the ecosystem that are amenable to an Eulerian approach.

Phytoplankton carbon is modelled as:

$$\frac{\partial P_C}{\partial t} = \frac{\partial}{\partial z} \left( K_z \frac{\partial P_C}{\partial z} \right) + \mu P_C - GP_C \quad (6)$$

where  $t$  (s) is time and  $z$  (m) is the vertical (positive upward) co-ordinate. The first term on the right of equation (6) describes vertical mixing by the turbulent eddy diffusivity,  $K_z$  (m<sup>2</sup> s<sup>-1</sup>), supplied by the physics model. The second term changes phytoplankton carbon in response to growth rate  $\mu$  (s<sup>-1</sup>). The maximum growth rate,  $\mu_m$  (s<sup>-1</sup>), is related to the temperature (following Eppley, 1972), modified by the cell nitrogen quota, by:

$$\mu_m = 1.16 \times 10^{-5} \left( \frac{Q - Q_{sub}}{Q_m - Q_{sub}} \right) 0.59 e^{0.0633T} \quad (7)$$

with  $Q_{sub}$  the subsistence cell quota and  $Q_m$  the maximum cell quota. The phytoplankton growth rate is then determined by the photosynthetically available radiation (PAR,  $I_{PAR}$ , W m<sup>-2</sup>) and accounting for respirative losses by

$$\mu = \mu_m \left( 1 - e^{-\left( \frac{\alpha I_{PAR} \theta}{\mu_m} \right)} \right) - r^B \quad (8)$$

(e.g. Geider et al., 1998) where  $\alpha$  (mg C (mg Chl)<sup>-1</sup> (W m<sup>-2</sup>)<sup>-1</sup> s<sup>-1</sup>) is the maximum light utilisation coefficient and  $\theta$  (mg Chl (mg C)<sup>-1</sup>) is a fixed phytoplankton Chlorophyll:carbon. The constant  $r^B$  (s<sup>-1</sup>) represents cell respiration. Photoinhibition of the growth rate at high irradiances has not been included. Such impacts are generally seen in samples incubated at constant, high light; at the thermocline and in mixing layers photoinhibition is unlikely to be a significant factor. Surface incident PAR is taken to be a fixed 45% of the solar irradiance. PAR decays exponentially away from the sea surface following

$$\frac{\partial I_{PAR}}{\partial z} = -I_{PAR} \left( k_{PAR} + \varepsilon \theta P_C \right) \quad (9)$$

with  $k_{PAR}$  ( $\text{m}^{-1}$ ) the attenuation coefficient for PAR and  $\varepsilon$  ( $\text{m}^2 (\text{mg Chl})^{-1}$ ) the Chlorophyll specific light extinction coefficient. The attenuation  $k_{PAR}$  can vary substantially through the year (higher during mixed conditions, lower in the surface stratified layer) and spatially (higher on the mixed side of a shelf sea front). This is incorporated by setting  $k_{PAR} = 0.12 \text{ m}^{-1}$  when the water column is mixed (determined by a surface-bottom temperature difference of less than  $0.25 \text{ }^\circ\text{C}$ ), and reducing to  $k_{PAR} = 0.09 \text{ m}^{-1}$  when the water is stratified. These values of  $k_{PAR}$  follow typical observations in the Celtic and Irish Seas (Bowers and Mitchelson-Jacob, 1996; Sharples et al., 2001). The final term on the right of equation (6) is a loss of phytoplankton to grazing. The grazing impact rate  $G$  ( $\text{s}^{-1}$ ) is taken as a constant throughout the year, set at a typical annual mean based on the observations of (Lee et al., 2002). At this stage it is noted that a number of important simplifications have been incorporated in the biological model, in particular a fixed (rather than temperature-dependent) respiration rate, a fixed Chl:C ratio, and a fixed grazing impact. While adding further biological processes may better reflect our understanding of the primary producers, they also require additional driving parameters that are generally poorly constrained by observational data. Justification of the validity of these simplifications in the context of the results of this work is included in the discussion.

Similar to equation (6), phytoplankton cellular nitrogen is modelled as:

$$\frac{\partial P_N}{\partial t} = \frac{\partial}{\partial z} \left( K_z \frac{\partial P_N}{\partial z} \right) + u P_C - G P_N \quad (10)$$

The second term on the right of equation (10) is the uptake of nitrogen, with the uptake rate a Michaelis-Menton function of the external dissolved inorganic nitrogen concentration  $DIN$  ( $\text{mmol m}^{-3}$ ), and the half saturation constant,  $k_u$  ( $\text{mmol m}^{-3}$ ):

$$u = \left[ u_m \left( 1 - \frac{Q}{Q_m} \right) \frac{S}{(k_u + S)} \right] + \begin{matrix} \mu Q : \mu < 0 \\ 0 : \mu \geq 0 \end{matrix} \quad (11)$$

with  $u_m$  ( $\text{mmol DIN} (\text{mg C})^{-1} \text{ s}^{-1}$ ) the maximum biomass-specific uptake rate. The last term in equation (11) describes dark respiration of cellular nitrogen. Finally external dissolved nitrogen is calculated as

$$\frac{\partial DIN}{\partial t} = \frac{\partial}{\partial z} \left( K_z \frac{\partial DIN}{\partial z} \right) - u P_C + e G P_N \quad (12)$$

with  $e$  the fraction of grazed phytoplankton cellular nitrogen recycled immediately back into the dissolved nitrogen pool. A flux of inorganic nitrogen from the seabed

acts to replenish water column nitrogen back to an initial winter concentration,  $DIN_0$  ( $\text{mmol m}^{-3}$ ):

$$\frac{\partial DIN_1}{\partial t} = \frac{f_{DIN}}{\Delta z} \left( 1 - \frac{DIN_1}{DIN_0} \right) \quad (13)$$

with  $DIN_1$  the dissolved nitrogen in the bottom depth cell of the model grid,  $\Delta z$  (m) the thickness of the model grid cell, and  $f_{DIN}$  ( $\text{mmol m}^{-2} \text{s}^{-1}$ ) the maximum flux of dissolved nitrogen from the seabed into the bottom depth cell. The value chosen (Table I) is based on the need to replenish water column nitrate within a reasonable time following autumnal re-mixing of a previously stratified water column. A typical post spring bloom flux into the bottom model grid cell is 5 - 10  $\mu\text{mol m}^{-2} \text{h}^{-1}$ , which is similar to the rates of Trimmer et al., 1999.

All of the parameters required by the model equations are listed in Table I. The typical ratio of  $S_2:M_2$  tidal current amplitudes in NW European shelf seas varies between 0.35 and 0.45 in regions that stratify in spring and summer, i.e. the Celtic Sea, the western English Channel, and the northern North Sea (S. Wakelin, Proudman Laboratory Liverpool, pers. comm.). A value of  $S_2:M_2=0.4$  is used for all model runs with a spring-neap cycle. The polarisation of the tidal current ellipses is fixed at a typical Celtic Sea value of  $-0.3$  (i.e. elliptical and anti-cyclonic).

| Parameter  | Symbol [units]   | Value                 |
|--|--|-----------------------|
| Total water column depth                             | $h$ [m]  | 80                    |
| Depth resolution                                     | $\Delta z$ [m]   | 1                     |
| PAR attenuation coefficient                          | $k_{PAR}$ [ $\text{m}^{-1}$ ]  | 0.09, 0.12            |
| Chlorophyll specific extinction coefficient          | $\varepsilon$ [ $\text{m}^2 (\text{mg Chl})^{-1}$ ]                                  | 0.0012                |
| Seabed nitrogen concentration                        | $DIN_0$ [ $\text{mmol m}^{-3}$ ]   | 7.0                   |
| Seabed nitrogen flux                                 | $f_{DIN}$ [ $\text{mmol m}^{-2} \text{s}^{-1}$ ]                                     | $1.16 \times 10^{-4}$ |
| Maximum growth rate                                  | $\mu_m$ [ $\text{s}^{-1}$ ]  | See equation (7)      |
| Quantum yield  | $\alpha$ [ $\text{mg C} (\text{mg Chl})^{-1} (\text{W m}^{-2})^{-1} \text{s}^{-1}$ ] | $4.63 \times 10^{-5}$ |
| Respiration rate                                     | $r^B$ [ $\text{s}^{-1}$ ]  | $1.39 \times 10^{-6}$ |
| Cellular Chl:carbon ratio                            | $\theta$ [ $\text{mg Chl} (\text{mg C})^{-1}$ ]                                      | 0.04                  |
| Maximum nitrogen uptake rate                         | $u_m$ [ $\text{mmol DIN} (\text{mg C})^{-1} \text{s}^{-1}$ ]                         | $9.26 \times 10^{-7}$ |
| Subsistence cell quota                               | $Q_{sub}$ [ $\text{mmol N} (\text{mg C})^{-1}$ ]                                     | 0.008                 |
| Maximum cell quota                                   | $Q_m$ [ $\text{mmol N} (\text{mg C})^{-1}$ ]   | 0.04                  |
| Half-saturation $DIN$ concentration                  | $k_u$ [ $\text{mmol DIN m}^{-3}$ ]   | 0.3                   |
| Grazing impact parameter                             | $G$ [ $\text{s}^{-1}$ ]  | $1.39 \times 10^{-6}$ |
| Proportion of recycled grazed phytoplankton nitrogen | $e$  | 0.5                   |

**Table I**  
Parameter values used by the model equations (6) – (13).

## Results

### *Timing of the spring bloom.*

As surface irradiance increases in spring the date at which the supply of heat can overcome the tidal mixing may vary depending on the phase of the spring-neap

cycle. This was investigated by identifying the time of the onset of the spring bloom (identified as the time when surface phytoplankton biomass exceeds a value of  $10 \text{ mg C m}^{-3}$ ) as a function of the phase lag of the  $S_2$  tidal currents relative to  $M_2$  at midnight on January 1<sup>st</sup>. Two examples are shown, one analogous to the central Celtic Sea with weak tidal currents ( $M_2$  amplitude of  $0.2 \text{ m s}^{-1}$ ; Fig. 2A), and one for stronger tidal currents closer to a shelf sea front ( $M_2$  amplitude of  $0.5 \text{ m s}^{-1}$ ; Fig. 2B). In both cases there is a clear fortnightly signal in the bloom onset as a function of phase lag. The gradually delayed spring tide currents initially force a similarly delayed the start of the bloom. The bloom timing then switches earlier as the preceding neap tide currents begin to allow stratification under weaker irradiance. For the case of weak tidal currents (Fig. 2A) the total range of the effect is 3 days. In the case of stronger tidal currents (Fig. 2B) the largest difference between the timings of established blooms is about 8 days. However, with the stronger tidal currents there is also the possibility of the initial stages of the bloom being eroded at spring tides (e.g. between phases of 1.4 and 3.2 radians, Fig. 2B) and leading to a late onset of the established bloom.

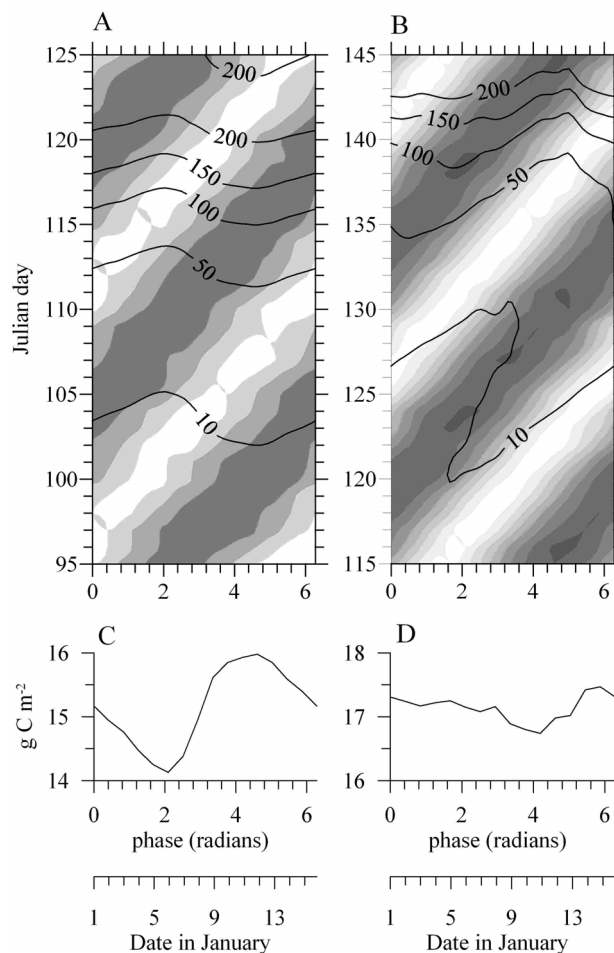


**Figure 2.**

Spring and early summer surface biomass (line contours,  $\text{mg C m}^{-3}$ ) and daily-averaged depth-mean currents (shaded) as a function of the January 1<sup>st</sup> phase (or time) difference between the  $M_2$  and  $S_2$  tidal constituents, for (A) a water depth of 80 m and  $M_2$  tidal current amplitude of  $0.2 \text{ m s}^{-1}$ , and (B) a water depth of 80 m and  $M_2$  tidal current amplitude of  $0.5 \text{ m s}^{-1}$ . Corresponding changes in the integrated carbon fixation from the start of the year to the peak of the spring bloom are shown in (C) and (D) for the  $M_2$  amplitudes of  $0.2$  and  $0.5 \text{ m s}^{-1}$  respectively. The shaded contouring illustrates neap tides (white) and spring tides (dark), contoured with a  $0.05 \text{ m s}^{-1}$  interval. Neap daily-averaged tidal currents are  $0.09 \text{ m s}^{-1}$  in (A) and  $0.27 \text{ m s}^{-1}$  in (B). The second x-axes below (C) and (D) allows interpretation of the phase difference in terms of the date of the first January spring tide.

The model also predicts a spring-neap effect on the total carbon fixed during the spring bloom. Integrating the gross carbon fixation up to the peak of the spring bloom in the low tidal current regime (Fig. 2C) shows there is a range of variability of almost  $2 \text{ g C m}^{-2}$ , about 14% of the mean. For the stronger tidal regime (Fig. 2D) this potential for inter-annual variability is less, with a total range of 4% compared to the mean.

*Spring-neap signals at a shelf sea front.*

Cross-frontal sections of temperature and phytoplankton biomass were simulated by combining, at each day through the year, model results from a series of runs with depth fixed at 80 metres and  $M_2$  tidal current amplitude allowed to vary from  $0.2$  to  $1.5 \text{ m s}^{-1}$  (e.g. Sharples and Simpson, 1996). The horizontal, cross-front dimension is quantified in terms of the stratification parameter  $\log_{10}(h/U^3)$  (Simpson and Hunter, 1974), with  $h$  (metres) the water depth and  $U^3$  ( $\text{m}^3 \text{ s}^{-3}$ ) the long-term average of the cubed depth-mean current speed. Resolution across the front in all the results is typically 0.04 units of  $\log_{10}(h/U^3)$ . Typical gradients of  $\log_{10}(h/U^3)$  in the vicinity of fronts in NW European shelf seas vary between 0.02 and  $0.06 \log_{10}(\text{m}^{-2} \text{ s}^3) \text{ km}^{-1}$  (Pingree and Griffiths, 1978). Spring-neap adjustment of fronts' positions has been observed to be 4 km (Simpson and Bowers, 1981), averaged over observed fronts in the Celtic and Irish Seas.

Cross-frontal sections for the case with the  $M_2$  tide only (Fig. 3A) and for neap and spring tides when  $M_2$  and  $S_2$  operate together (Fig. 3B, C) show typical features of tidal mixing fronts. Isotherms of the thermocline reach upward to form a sharp surface front, and downward to form a weaker bottom front. The position of the edge of the front (determined by a surface-bottom temperature difference of  $1^\circ\text{C}$ ) occurs at  $\log_{10}(h/U^3) = 2.75 - 2.8$  for the spring tide and  $M_2$  fronts respectively, and  $\log_{10}(h/U^3) = 2.4$  for the neap tide front. Observed frontal positions tend to average at about  $\log_{10}(h/U^3) = 2.7$  (Holt and Umlauf, in press). All three fronts in Fig. 3 show enhanced phytoplankton biomass within the front at the surface, and decreasing concentrations within the thermocline on the stratified side of the front. With the 1-D framework used to generate the fronts, this indicates that increased frontal surface biomass can be driven by the weaker stratification providing a flux of nutrients to the surface, at the same time as maintaining sufficient near-surface stability for the phytoplankton to be able to photosynthesise (Loder and Platt, 1985). There is a marked difference between the spring tide (Fig. 3B) and neap tide (Fig. 3C) fronts. At neap tide stratification extends into lower  $\log_{10}(h/U^3)$ , with a broader frontal signature in phytoplankton biomass and higher concentrations of biomass (maximum surface concentrations of  $240 \text{ mg C m}^{-3}$  at neap tide compared to  $190 \text{ mg C m}^{-3}$  at spring tide).

The repeatability of this apparent neap-spring physical adjustment of frontal position and the corresponding contrasts in frontal biomass can be seen by considering the seasonal behaviour of stratification and surface biomass (Fig. 4). The amplitude of the spring-neap frontal excursion ranges between 0.2 and 0.35  $\log_{10}(h/U^3)$ , suggesting horizontal excursions of between 3 and 17 km based on the

typical gradients of  $\log_{10}(h/U^3)$  and a mean over the stratified period of about 4 – 13 km.

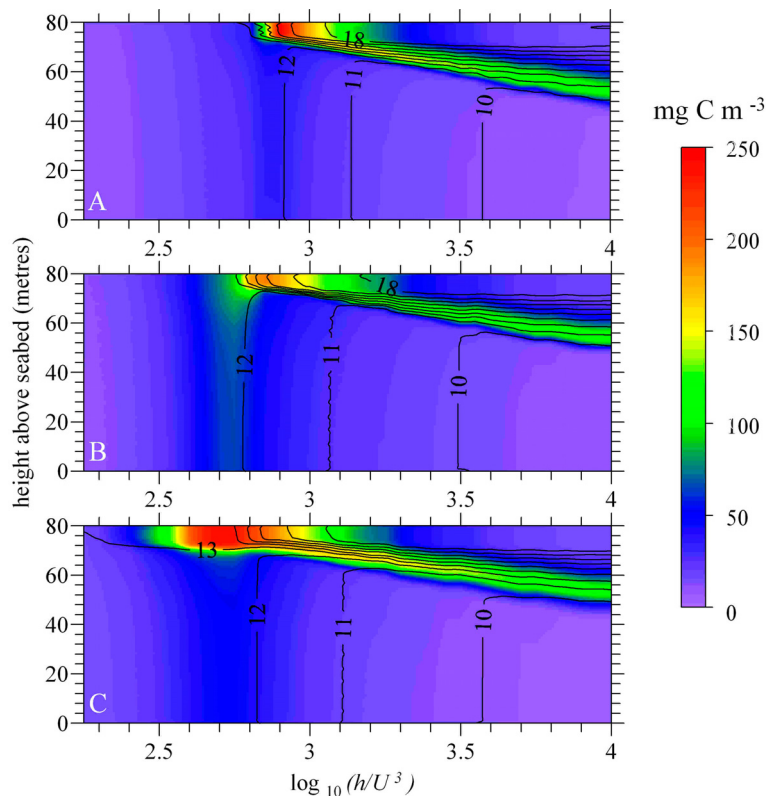


**Figure 3.**

Cross-frontal slices of temperature (lines) and phytoplankton carbon (colours) for (A) the model with  $M_2$  tides only on Julian day 182, (B) the model with a spring-neap cycle for Julian day 182 (spring tides), and (C) the model with a spring-neap cycle for Julian day 189 (neap tides).

This ranges higher than the mean adjustment of 4 km reported by Simpson and Bowers, 1981, probably because the 1-dimensional method does not allow dynamic adjustment of the density gradients at the front which would limit the extent of neap re-stratification. The timing and contrasts in vertical structure are, however, correctly re-produced. For the case with the  $M_2$  tide only (Fig. 4A) there is a smooth transition from the spring bloom to an established frontal biomass that gradually decays after mid summer. Indeed, Fig. 4A suggests that one interpretation of the existence of frontal primary productivity is that the weak frontal stratification effectively maintains a localised spring bloom-like environment through the summer. For the case with a spring-neap tidal cycle (Fig. 4B) there is a band approximately between  $2.4 < \log_{10}(h/U^3) < 2.8$  that undergoes a fortnightly series of biomass pulses between the end of May and the end of August. The dynamics underlying this spring-neap pulsing of surface biomass are similar to those at the spring bloom. Stratification begins as the tidal currents reduce towards neap tides, allowing the surface heat flux to overcome the available mixing, and is then rapidly eroded as the tidal currents increase again towards spring tides (Fig. 5A). Peak stratification occurs about 3 days after neap tides. The phytoplankton biomass at the surface rises with the developing stratification reaching it maximum also about 3 days after neaps (Fig. 5B). At the same time the surface nitrate, previously replenished by the strong vertical mixing at spring tides, is reduced though not completely depleted (Fig. 5B).

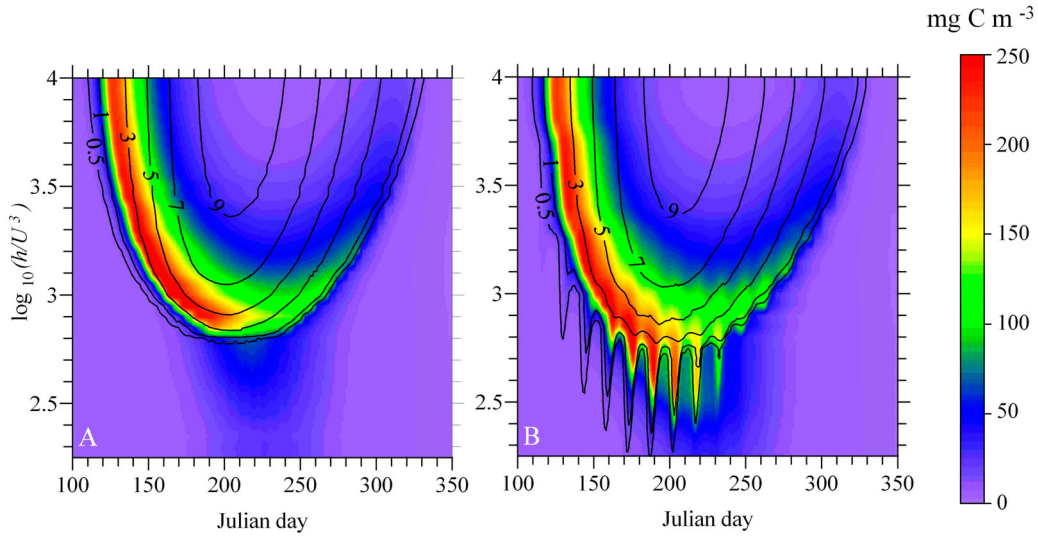


**Figure 4.**

Variations of cross-front surface phytoplankton carbon (colours) and surface-bottom temperature difference (lines) from early spring to late autumn for (A) the model with  $M_2$  tides only, and (B) the model with a spring-neap cycle.

The absolute uptake of the surface nitrate is locked to the increase in biomass, while the biomass-specific uptake of nitrate has a broader distribution lagging the neap tide by about 2 days (Fig. 5C). The absolute rate of surface carbon fixation peaks at  $0.07 \text{ g C m}^{-3} \text{ d}^{-1}$  1 day after the peak biomass, compared to a minimum of  $0.02 \text{ g C m}^{-3} \text{ d}^{-1}$  over the previous spring tide. The biomass-specific carbon fixation reduces slightly as the stratification develops and has a sharp peak just as the stratification is eroded (Fig. 5D). This peak is due to the addition of biomass with high nitrate quota from below the transient surface layer briefly growing efficiently in the decaying stratification. The small reduction in the efficiency of carbon fixation indicates growth exceeding the capacity for nitrate uptake, leading to a reduction in the cellular nitrate quota. Overall, the small delay in the timing of stratification, peak nitrate uptake, and peak biomass, indicates that the rate of stratification is governing the capacity of the biological components to respond to the environment.

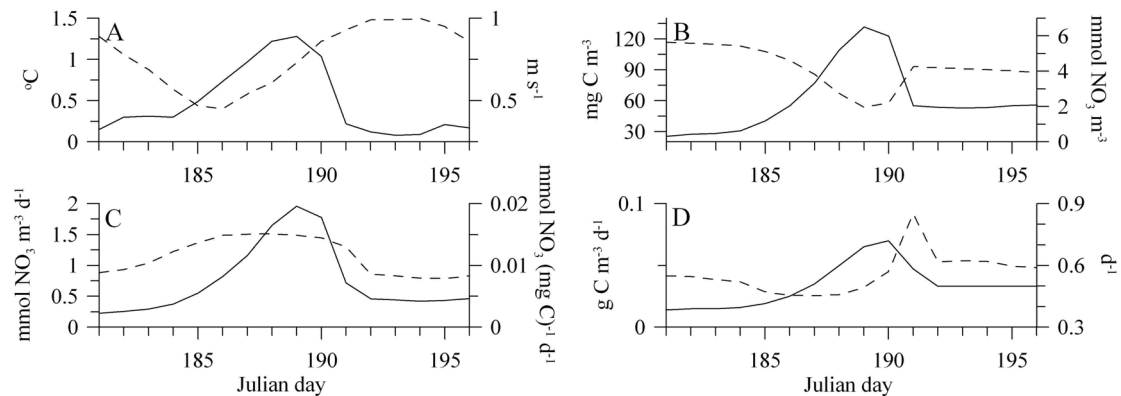


**Figure 5.**

Time series over one spring neap cycle of (A) surface-bottom temperature difference (solid line) and daily-averaged depth-mean current speed (dashed line), (B) surface phytoplankton (solid line) and surface  $DIN$  (dashed line), (C) absolute surface nitrate uptake rate (solid line) and biomass-specific surface nitrate uptake (dashed line), and (D) absolute rate of surface carbon fixation (solid line) and biomass-specific surface growth rate (dashed line). In each panel the solid line uses the left axis, and the dashed line uses the right axis.

### Spring-neap signals in the summer thermocline.

Below the sea surface the spring-neap cycle in bottom boundary layer turbulence has clear impacts on the thermocline layer of phytoplankton. The base of the thermocline is periodically eroded as the tidal turbulence increases towards spring tides. As neap tides approach the strength of turbulence high in the water column decreases, allowing the thermocline to develop deeper in the water column (Fig. 6A). The total vertical excursion of this thermocline movement is about 3 m. The highest position of the thermocline base occurs at the same time as spring tides, while the deepest position occurs about 2 days after neap tides. The biological response has a clear sequence. The region of peak nitrate uptake tracks the base of the thermocline, with maximum values tending to occur approaching and during spring tides (Fig. 6B), a consequence of both increased mixing and a sharpening of the nitracline. Maximum biomass-specific carbon fixation rates, reaching  $0.40 \text{ d}^{-1}$  (compared to a neap tide minimum of  $0.32 \text{ d}^{-1}$ ) occur at spring tides (Fig. 6C). This is partially due to the supply of nitrate (increasing the cell nitrogen quota) but also because of the increased light available for photosynthesis in the shallower thermocline base. Pulses in thermocline biomass occur at or just after neap tides (Fig. 6D), typically reaching  $140 \text{ g C m}^{-3}$ , compared to spring tide minima of about  $100 \text{ mg C m}^{-3}$ . The flux of this organic carbon out of the thermocline peaks at  $200 \text{ mg C m}^{-2} \text{ d}^{-1}$  at the midpoint between neap and spring tides (Fig. 6E), with a broader minimum flux of  $25 - 50 \text{ mg C m}^{-2} \text{ d}^{-1}$  around neap tides. By contrast, at the same time of year the mean carbon flux with just the  $M_2$  tide is about  $100 \text{ mg C m}^{-2} \text{ d}^{-1}$ .

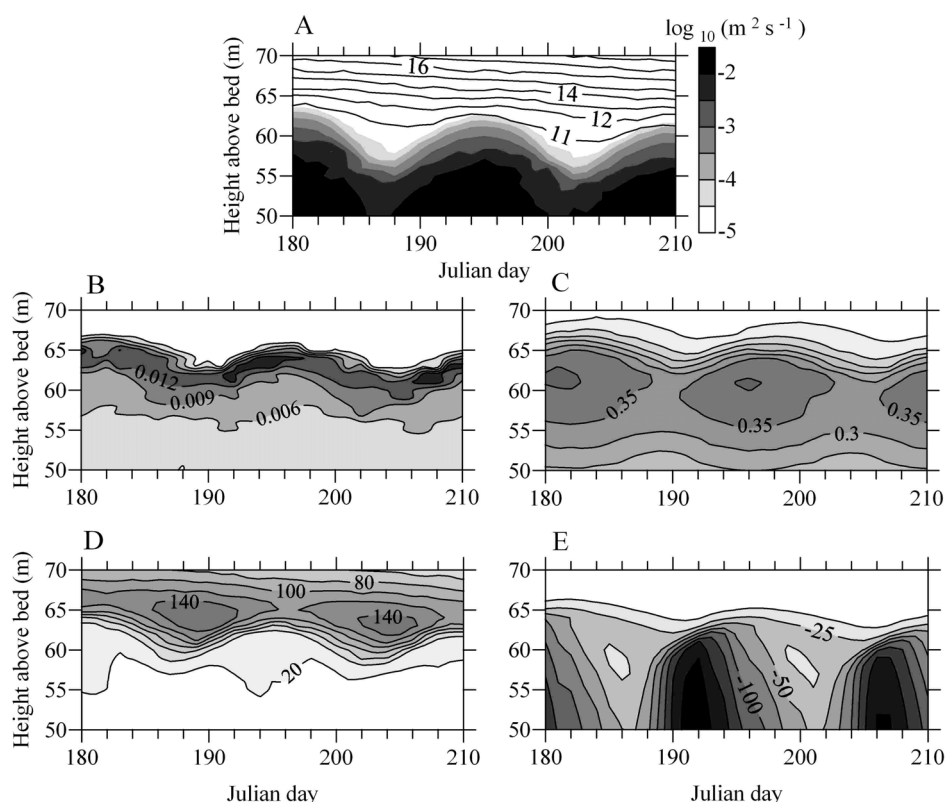


**Figure 6.**

Spring-neap variability in the thermocline. The physical variability is shown as changes in the temperature structure (line contours, °C) and vertical eddy diffusivity (shaded) in (A), with spring tides occurring on Julian day 195, neaps tides on Julian days 187 and 202. The corresponding biological signals are (B) nitrate uptake rate ( $\text{mmol DIN} (\text{mg C})^{-1} \text{ d}^{-1}$ ), (C) specific growth rate ( $\text{d}^{-1}$ ), (D) phytoplankton biomass ( $\text{mg C m}^{-3}$ ), and (E) vertical carbon flux ( $\text{mg C m}^{-2} \text{ d}^{-1}$ ).

## Discussion and Conclusions

The results indicate clear impacts of the spring-neap cycle on a range of aspects of primary production in thermally-stratifying shelf seas. The following discussion will place the results in the context of other causes of variability, and quantify the consequences of the modelled variability in terms of potential impacts on estimating annual production and carbon export in shelf seas. Throughout it is advisable to be wary of over-interpreting absolute values of, for instance, total annual production or annual carbon export because of the simplicity of the modelled ecosystem. However, given the difficulty in obtaining sufficiently long and well-resolved time series of phytoplankton production sufficient to address the impacts of both meteorological and tidal variability, this modelling approach provides a viable means of making a first estimate of the proportionate impact of the spring-neap cycle on primary production, and provides a basis for placing typically “snapshot” observations of production rates into a longer-term context. This discussion begins with some demonstrations that the absolute predictions made by the model do compare favourably with typical observations, providing some level of support for the use of such a simple biological model. Most of the interpretation that then follows makes comparisons between the model using  $M_2$  tides only and using a realistic spring-neap cycle. Estimates of the likely impacts of key biological simplifications are also provided.

Comparison between the modelled production rates and fluxes, and typical observations, provides support for the coupled 1-dimensional framework. The total annual production predicted by the model for a site analogous to the central, seasonally stratifying Celtic Sea is about  $70 \text{ g C m}^{-2}$ ; the observed annual rate of primary production has been reported as  $80 \text{ g C m}^{-2}$  (Joint and Groom, 2000). The success of this model result reflects the dominant role of the initial winter nitrate concentration in fuelling the spring bloom and in setting the limits of the vertical nitrate gradient at the base of the thermocline in summer. The vertical turbulent flux of nitrate into the summer thermocline predicted by the model was typically  $2 - 3 \text{ mmol NO}_3 \text{ m}^{-2} \text{ d}^{-1}$  during the transition between neap and spring tides, compared to direct measurements of  $2 \pm 1 \text{ mmol NO}_3 \text{ m}^{-2} \text{ d}^{-1}$  (Sharples et al., 2001). This comparison in particular reflects the model’s skill in simulating the turbulent diffusivity at the base of the thermocline, along with setting the strength of the vertical nitrate gradient (a function of both the thermocline turbulence and the phytoplankton nitrate uptake).

The timing of the spring bloom was shown to vary in response to the timing of spring tides during the increasing surface irradiance that drives stratification (Fig. 2). In the case of weak tidal currents ( $M_2$  amplitude of  $0.2 \text{ m s}^{-1}$ ) the model predicts that this could lead to inter-annual variability in the timing of the spring bloom of up to 3 days (Fig. 2A). With real meteorological forcing the spring bloom in the northern North Sea has been predicted to vary over a window of about 1 month, with a standard deviation of 6 days (Sharples et al., 2006), and so the spring-neap cycle contributes only about 10% of the total variability with the rest dominated by the meteorology. However, in a more transitional environment where stronger tidal currents lead to a later onset of thermal stratification ( $M_2$  amplitude of  $0.5 \text{ m s}^{-1}$ ; Fig. 2B), the range of the possible spring-neap changes to the start of the bloom was predicted to be 8 days. For the northern North Sea this could account for almost 25% of the total inter-annual variability. With the timing of the bloom being an important

determinant of the survival of other components of the marine ecosystem (e.g. Head et al., 2000; Platt et al., 2003; Frederiksen et al., 2006), an assessment of variability solely in response to meteorological forcing will not be sufficient.

There were small changes in the total primary production achieved by the spring bloom as a function of the spring-neap cycle (Fig. 2C, D). In this simple biological model the production of the spring bloom is primarily set by the nitrate available in the surface layer as stratification first develops. However, variations in bloom production do occur in response to the rate at which the stratification develops. In the low tidal regime the minimum bloom production occurs when the bloom is triggered late. This is not the result of a shorter growth period; the integration for the bloom productivity is taken to the peak of the spring bloom, rather than a fixed date. For the delayed bloom the slightly faster rate of increase in the strength of the stratification, due to the higher surface irradiance, is more efficient at shutting off the supply of nitrogen from the bottom layer and so limiting the total nitrate supply to the surface layer phytoplankton, a plausible mechanism for affecting bloom productivity and worthy of further consideration. In the case of higher tidal currents most of the change in bloom production is associated with the early bloom onset and the temporary erosion of the initial stages of the spring bloom by spring tides.

The frontal biomass for the M<sub>2</sub> case, and within the corresponding region of sustained stratification for the spring-neap case, was very similar (Fig. 4). The important result for the spring-neap front is the additional region of periodic stratification in response to the cyclic tidal mixing, leading to marked fortnightly pulses of surface phytoplankton biomass dynamically similar to the processes that drive the main spring bloom. Primary production rates within the surface waters affected by this spring-neap adjustment varied between 0.02 and 0.07 g C m<sup>-3</sup> d<sup>-1</sup>, with the resulting excursion region surface biomass varying typically between 70 and 250 mg C m<sup>-3</sup>. This frontal production is fuelled by nitrate mixed towards the surface at spring tides. The model predicts surface nitrate to vary from <0.5 mmol m<sup>-3</sup> at neap tides to between 1 and 3 mmol m<sup>-3</sup> at springs, suggesting a mean nitrate flux to the surface 10 m of between 0.7 – 3.6 mmol m<sup>-2</sup> d<sup>-1</sup> over the 7 days between neap and spring tides. This agrees with an estimate made by Loder and Platt, 1985; taking the modelled adjustment region to be 4 – 13 km, then their estimate of 0.12 mmol m<sup>-1</sup> s<sup>-1</sup> suggests a vertical flux within the adjustment region of 0.8 – 2.5 mmol m<sup>-2</sup> d<sup>-1</sup>. Possible observational evidence for fortnightly pulsing of phytoplankton biomass is limited. Weekly surveys of the front in the western Irish Sea (Richardson et al., 1985) have showed frontal surface chlorophyll in early summer ranging between <2 to >4 mg m<sup>-3</sup> consistent with spring-neap variability. The model predicts a range of about 3 – 10 mg Chl m<sup>-3</sup>; the relative change in biomass is the same as the observations, though the discrepancy in the absolute values could arise from the value used for the constant C:Chl in the model. A fortnightly signal in phytoplankton concentrations at a front has also been reported over the Kashevarov Bank in the Sea of Okhotsk (Rogachev et al., 2001). The factor of 10 difference between the spring and neap tide currents over the Bank means that a direct comparison of changes in phytoplankton biomass with the model is unlikely to be reliable. However, a speculation of Rogachev et al., 2001, is that the dominance of a particular species of copepod over the Bank may arise because the timing of its life history is ideal for exploiting the regular fortnightly pulses in phytoplankton biomass. The present model does not include the possibility of such “biological resonance” in the grazers, and it remains an

intriguing possibility for shelf sea fronts that vary with fixed, tidally-driven cycles in stability and primary production.

The 1-dimensional model accounts for the increasing vertical exchange approaching a front, and the role of spring-neap modulation of vertical mixing in adjusting the front's position. However, it cannot account for eddy exchange across the front or the weak cross-frontal friction-driven exchange driven by the residual flows. Loder and Platt, 1985, estimated that local vertical exchange and spring-neap adjustment could account for 80% of the nitrate demands at the front, with the two neglected advective processes supplying the remaining 20%. There is no clear understanding of how either of these two processes might respond to the spring-neap cycle, but with their relatively minor role in frontal nitrate supply the errors in the model comparisons are expected to be small.

The impacts of repeated blooms on the annual productivity of the front can be assessed in the model by comparing the cross-frontal integrated annual production with just the  $M_2$  tide operating and with the spring-neap cycle (Fig. 7). With a spring-neap cycle, there is a clear overall increase in annual primary production at the position of the front compared to with the  $M_2$  tide only (Fig. 7A). At the mean position of the front of  $\log_{10}(h/U^3) = 2.75$  the effect of the spring-neap cycle is to add about 50% to the annual primary production. Within the adjustment region (between  $2.4 < \log_{10}(h/U^3) > 2.75$ ) the spring-neap cycle results in an average increase in annual carbon fixation of about 70% above that of the  $M_2$  tide only. Within the frontal region there is a comparable increase in the downward supply of carbon (Fig. 7B), as the spring tide remixing events redistribute the growth achieved during the last neap tide stratification. Clearly the spring-neap cycle could play an important role in the primary production of shelf sea fronts. Any assessment of frontal ecosystems, both pelagic and benthic, may need to include variability in the tidal mixing both as a driver of significant extra primary productivity and as a source of regular variability in the surface concentrations of phytoplankton and downward fluxes of organic carbon.

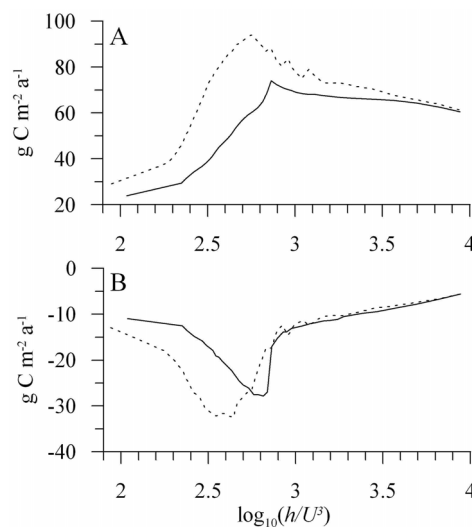


**Figure 7.**

The impact of the spring-neap cycle on (A) annual carbon fixation and (B) annual vertical carbon flux from mixed (low  $\log_{10}(h/U^3)$ ) to stratified (high  $\log_{10}(h/U^3)$ ) shelf waters. The solid line is for the model run with  $M_2$  tides only, and the dashed line is for the model with a spring-neap cycle.

On the stratified side of the tidal mixing front the modelled cycle of spring-neap changes in thermocline erosion and deepening are consistent with the suggestions of Sharples et al., 2001. Variability in primary production rates within the thermocline is partially driven by spring-neap changes in the supply of nitrate (both because of the changes in mixing and in the strength of the vertical nitrate gradient), and also by the vertical excursion of the base of the thermocline through the light gradient (Fig. 6C). Pulses in thermocline biomass are predicted 1- 2 days after neap tides and appear to be curtailed by increased mixing in the bottom layer. The fortnightly modulation of thermocline growth rate resulted in almost 30% additional growth at spring tides compared to neaps. This is less than the factor of 2 difference in growth potentially driven by fluctuations in surface irradiance between cloudy and sunny days (Sharples et al, 2007), but it is still a potentially significant and predictable source of variability in thermocline primary production. The periodic erosion of the base of the thermocline leads to fortnightly variations in the flux of carbon into the bottom mixed layer (Fig. 6E), ranging between about 50 and 200 mg C m<sup>-2</sup> d<sup>-1</sup>, with the maximum fluxes occurring as the tidal currents increase towards spring tides. Assessing the integrated annual impact of the spring-neap cycle in a stratified region (Fig. 8) indicates that much of the apparently strong fortnightly signals in growth and carbon export are averaged out over the year. On the stratified side of the front ( $\log_{10}(h/U^3) > 2.9$ ) there is a small increase in annual primary production (Fig. 8A), with spring-neap carbon production being about 15% higher than with the M<sub>2</sub> tide only. This increase in production decreases away from the front, with the spring-neap and M<sub>2</sub> models predicting similar annual primary production above  $\log_{10}(h/U^3) = 3.6$ . Taking the stratified Celtic Sea as an example, the mean depth is about 110 metres and, with M<sub>2</sub> and S<sub>2</sub> tidal current amplitudes of 0.35 and 0.14 m s<sup>-1</sup> respectively, the mean cubed tidal currents is about 0.025 m<sup>3</sup> s<sup>-3</sup>. Hence  $\log_{10}(h/U^3)$  is typically 3.6, suggesting that spring-neap effects on the annual primary production of the region are not significant. Based on the typical gradients of  $\log_{10}(h/U^3)$ , the limitation of the effects of the spring-neap cycle to  $\log_{10}(h/U^3) < 3.6$  would suggest the impacts to be local within a horizontal distance of 15 – 50 km on the stratified side of the front. There is no significant difference between the spring-neap and M<sub>2</sub> predictions in annual fluxes of carbon out of the thermocline (Fig. 8B) away from the influence of the front. Thus for primary production and carbon fluxes associated with the shelf sea seasonal thermocline, the importance of the spring-neap cycle may primarily be in terms of fortnightly variability in thermocline biomass and pulses in the flux of carbon to the bottom layer. Overall, at the front and within the stratified waters, the spring-neap response of the biological system is a consequence of the timescales of carbon fixation (e.g. turnover timescales of typically 2 days) allowing phytoplankton to take advantage of the 7 days between extremes of mixing in the spring-neap cycle. It should be emphasised that these predictions for spring-neap variability within the shelf sea seasonal thermocline are speculative; there are no direct observations of rates of primary production nor carbon export sufficient to resolve the spring-neap cycle.

All the above results and the validity of their interpretation rely on the applicability of the model. The biological model in particular has been kept simple;

adding complexity to any ecosystem model always brings with it extra controlling parameters that are very often poorly constrained by observations. An implicit assumption in the interpretation of the results is that errors arising from model simplifications are similar for both the model with  $M_2$  tide only and for the model with the spring-neap cycle; i.e. in comparing the two model runs the errors cancel sufficiently to leave a reliable result. For instance, the modelled phytoplankton were given a fixed respiration rate (equation (8)), rather than a temperature-dependent rate. This could result in errors in parts of the water column where the spring-neap cycle produces markedly different temperatures. Within the region of the spring-neap frontal adjustment the surface temperature varies between about  $12^\circ\text{C}$  and  $13^\circ\text{C}$ , compared to a temperature of  $12^\circ\text{C}$  for the water adjacent to the front with the  $M_2$  tide only (Fig. 3). On the stratified side of the front surface temperatures are generally identical for both model runs, but at the base of the thermocline there is a narrow region where the temperature oscillates by  $\pm 0.5^\circ\text{C}$  in response to the spring-neap cycle. Using a Q10 description of phytoplankton respiration, with Q10 between 4 and 9 (Lefevre et al., 1994) and a temperature change of  $1^\circ\text{C}$ , suggests a change in respiration rate of 15 – 25%. The biggest impact would be surface production in the spring-neap adjustment region. Assuming a growth rate of  $1\text{ d}^{-1}$  and the modelled respiration rate of  $0.12\text{ d}^{-1}$  changing by 25% results in the growth-respiration balance changing by only 4%, which is negligible compared to the predicted contrast in primary production generated by the spring-neap cycle (Fig. 7A). At the base of the thermocline, taking a growth rate of typically  $0.25\text{ d}^{-1}$  suggests a potential oscillation in the growth-respiration balance of 30%. However, the base of the thermocline contributes only about 10% to the water column primary production (Fig. 6D), so the error associated with the fixed respiration rate here will be  $<4\%$ .

A second source of potential error is the fixed Chl:C ratio. This ratio has been seen to change by up to a factor of 4 in the Celtic Sea, ranging from  $0.04 - 0.03\text{ mg Chl (mg C)}^{-1}$  in the thermocline and bottom mixed layer,  $0.02\text{ mg Chl (mg C)}^{-1}$  in vertically-mixed regions,  $0.02 - 0.01\text{ mg Chl (mg C)}^{-1}$  at a tidal mixing front, and  $0.01\text{ mg Chl (mg C)}^{-1}$  at the surface of a stratified water column (Holligan et al., 1984). The value of  $0.04\text{ mg Chl (mg C)}^{-1}$  used by the model is typical for the summer thermocline and for the pre-spring bloom mixed water column, regions which dominate the annual primary production and so contributing to the agreement with observed Celtic Sea annual primary production rates. Lower Chl:C is likely to occur in surface waters during summer, either in the stratified region or in the frontal transition region, and tend to reduce the primary production. The surface layer of the stratified region is not a concern, partially because production in the thermocline dominates (Fig. 6D) and also because the error would affect both the  $M_2$  and spring-neap runs similarly. Of potentially more significance is the fortnightly production predicted within the frontal transition region. Taking a summer surface PAR of  $80\text{ W m}^{-2}$  distributed exponentially over the 10 m surface layer (a mean surface layer irradiance of  $50\text{ W m}^{-2}$ ), then equation (8) suggests the effect of reducing Chl:C by a factor of 2 – 4 is to reduce the growth rate by about 5 – 10%, so the error is significantly less than the contrast in frontal production between the  $M_2$  and the spring-neap model runs (Fig. 7A).

A final possible source of error is the simplification of a fixed grazing impact, which might normally be expected to vary seasonally (Lee et al., 2002). Changes in grazing impact might affect the model results of primary production within regions

where there is marked spring-neap variability in biomass, i.e. the frontal transition region and the summer thermocline. Some additional runs of the model were carried out to assess this, comparing  $M_2$  and spring-neap results using a grazing impact that follows a seasonal cycle (see Fig. 4 of Lee et al., 2002). The results discussed earlier (Fig. 7) are quantitatively robust to this change in the treatment of grazing, both showing the region of additional annual carbon fixation caused by spring-neap frontal transition, and the increased production within the thermocline generated by the spring-neap cycle up to  $\log_{10}(h/U^3) = 3.6$ .

In conclusion, a model-based experiment has shown small but potentially significant effects of the spring-neap contrast of tidal mixing on the timing of the spring bloom, the primary production achieved by the bloom, and on the growth within, and downward carbon export from, the seasonal thermocline. These results are broadly robust to key simplifications within the biological model. Any study of the inter-annual variability in shelf sea primary production should consider that it is not only variability in meteorological forcing that may be driving the ecosystem. The strongest impacts of the fortnightly mixing variability occur within 15 – 50 km of the shelf sea tidal mixing fronts. Given the ecological importance of frontal regions as localised sources of organic fuel for the summer marine ecosystem, this has implications for the minimum horizontal resolution required in 3-dimensional coupled physics-ecosystem models of shelf systems. The impacts of the spring-neap cycle on these regions is partially the result of the transitional stratification being more susceptible to modulated mixing, but also because the time scale of the spring-neap cycle is suited to the response times inherent within the primary production. The model results are partially supported by available observations. However, further work is required to assess the viability of the predictions, and to investigate the potential for regular physical forcing of the primary production having impacts at higher trophic levels.

### **Acknowledgements**

In developing this modelling approach and its interpretation I have benefited greatly from many fruitful discussions on biological-physical interactions with John Simpson (University of Wales, Bangor), and Patrick Holligan and Mark Moore (University of Southampton). Jason Holt (Proudman Oceanographic Laboratory) provided helpful advice on the implementation of the turbulence model. Thanks to the anonymous referees for thought-provoking critiques. This work was funded by the UK Natural Environment Research Council (Oceans 2025 core funding to the Proudman Oceanographic Laboratory).

### **References**

- Allen, J. I., Siddorn, J. R., Blackford, J. C., and Gilbert, F. J. (2004). Turbulence as a control on the microbial loop in a temperate seasonally stratified marine systems model. *Journal of Sea Research*, **52(1)**, 1-20.
- Balch, W. M. (1986). Are red tides correlated to spring-neap tidal mixing?: use of a historical record to test mechanisms responsible for dinoflagellate blooms. In: Bowman, M. J., Barber, R. T., and Mooers, C. N. K. (eds.), *Tidal Mixing and Plankton Dynamics*, Springer-Verlag, New York, 193-223.

- Bowers, D. G., and Mitchelson-Jacob, E. G. (1996). Inherent optical properties of the Irish Sea determined from underwater irradiance measurements. *Estuarine Coastal and Shelf Science*, **43(4)**, 433-447.
- Burchard, H., Petersen, O., and Rippeth, T. P. (1998). Comparing the performance of the Mellor-Yamada and the k-epsilon two-equation turbulence models. *Journal of Geophysical Research*, **103(C5)**, 10543-10554.
- Canuto, V. M., Howard, A., Cheng, Y., and Dubovikov, M. S. (2001). Ocean turbulence. Part I: One-point closure model - Momentum and heat vertical diffusivities. *Journal of Physical Oceanography*, **31(6)**, 1413-1426.
- Droop, M. R. (1974). Nutrient status of algal cells in continuous culture. *Journal of the Marine Biological Association of the United Kingdom*, **54(4)**, 825-855.
- Durazo, R., Harrison, N. M., and Hill, A. E. (1998). Seabird observations at a tidal mixing front in the Irish Sea. *Estuarine Coastal and Shelf Science*, **47(2)**, 153-164.
- Eppley, R. W. (1972). Temperature and phytoplankton growth in the sea. *Fishery Bulletin*, **70(4)**, 1063-1085.
- Eslinger, D. L. and Iverson, R. L. (2001). The effects of convective and wind-driven mixing on spring phytoplankton dynamics in the Southeastern Bering Sea middle shelf domain. *Continental Shelf Research*, **21(6-7)**, 627-650.
- Frederiksen, M., Edwards, M., Richardson, A. J., Halliday, N. C., and Wanless, S. (2006). From plankton to top predators: bottom-up control of a marine food web across four trophic levels. *Journal of Animal Ecology*, **75(6)**, 1259-1268.
- Geider, R. J., MacIntyre, H. L., and Kana, T. M. (1998). A dynamic regulatory model of phytoplanktonic acclimation to light, nutrients, and temperature. *Limnology and Oceanography*, **43(4)**, 679-694.
- Head, E. J. H., Harris, L. R., and Campbell, R. W. (2000). Investigations on the ecology of *Calanus* spp. in the Labrador Sea. I. Relationship between the phytoplankton bloom and reproduction and development of *Calanus finmarchicus* in spring. *Marine Ecology-Progress Series*, **193**, 53-73.
- Holligan, P. M., Harris, R. P., Newell, R. C., Harbour, D. S., Head, R. N., Linley, E. A. S., Lucas, M. I., Tranter, P. R. G., and Weekley, C. M. (1984). Vertical distribution and partitioning of organic carbon in mixed, frontal and stratified waters of the English Channel. *Marine Ecology Progress Series*, **14**, 111-127.
- Holt, J., and Umlauf, L. Modelling the tidal mixing fronts and seasonal stratification of the Northwest European Continental shelf. *Continental Shelf Research*, in press.
- Horne, E. P. W., Loder, J. W., Naimie, C. E., and Oakey, N. S. (1996). Turbulence dissipation rates and nitrate supply in the upper water column on Georges Bank. *Deep-Sea Research Part II*, **43(7-8)**, 1683-1712.
- Joint, I., and Groom, S. B. (2000). Estimation of phytoplankton production from space: current status and future potential of satellite remote sensing. *Journal of Experimental Marine Biology and Ecology*, **250(1-2)**, 233-255.
- Lee, J. Y., Tett, P., Jones, K., Luyten, P., Smith, C., and Wild-Allen, K. (2002). The PROWQM physical-biological model with benthic-pelagic coupling applied to the northern North Sea. *Journal of Sea Research*, **48(4)**, 287-331.
- Lefevre, D., Bentley, T. L., Robinson, C., Blight, S. P., and Williams, P. J. L. (1994). The temperature response of gross and net community production and respiration in time-varying assemblages of temperate marine micro-plankton. *Journal of Experimental Marine Biology and Ecology*, **184(2)**, 201-215.

- Loder, J. W. and Platt, T. (1985). Physical controls on phytoplankton production at tidal fronts. In: Gibbs, P. E. (ed.), *Proceedings of the 19th European Marine Biology Symposium*, Cambridge University Press, 3-21.
- Lough, R. G. and Manning, J. P. (2001). Tidal-front entrainment and retention of fish larvae on the southern flank of Georges Bank. *Deep-Sea Research Part II* **48(1-3)**, 631-644.
- Maguer, J. F., L'Helguen, S., and Le Corre, P. (2000). Nitrogen uptake by phytoplankton in a shallow water tidal front. *Estuarine Coastal and Shelf Science*, **51(3)**, 349-357.
- McGillicuddy, D. J. (1995). One-dimensional numerical simulation of primary production: Lagrangian and Eulerian formulations. *Journal of Plankton Research*, **17(2)**, 405-412.
- New, A. L. (1988). Internal tidal mixing in the Bay of Biscay. *Deep-Sea Research A*, **35(5)**, 691-709.
- Patel, V. C., Rodi, W., and Scheuerer, G. (1985). Turbulence models for near-wall and low reynolds-number flows - a review. *AIAA Journal*, **23(9)**, 1308-1319.
- Pingree, R. D. and Griffiths, D. K. (1978). Tidal fronts on shelf seas around the British Isles. *Journal of Geophysical Research*, **83**, 4615-4622.
- Pingree, R. D., Holligan, P. M., Mardell, G. T. and Head, R. N. (1976). Influence of physical stability on spring, summer and autumn phytoplankton blooms in Celtic Sea. *Journal of the Marine Biological Association of the United Kingdom*, **56(4)**, 845-873.
- Pingree, R. D. and Mardell, G. T. (1981). Slope turbulence, internal waves and phytoplankton growth at the Celtic Sea shelf-break. *Philosophical Transactions of the Royal Society of London*, **A302**, 663-682.
- Pingree, R. D., Pugh, P. R., Holligan, P. M. and Forster, G. R. (1975). Summer phytoplankton blooms and red tides along tidal fronts in approaches to English Channel. *Nature*, **258**, 672-677.
- Platt, T., Fuentes-Yaco, C., and Franks, K. T. (2003). Spring algal bloom and larval fish survival. *Nature*, **423**, 398-399.
- Probyn, T. A., Mitchellinnes, B. A., and Searson, S. (1995). Primary productivity and nitrogen uptake in the subsurface chlorophyll maximum on the eastern Agulhas Bank. *Continental Shelf Research*, **15(15)**, 1903-1920.
- Richardson, K., Lavin-Peregrina, M. F., Mitchelson, E. G., and Simpson, J. H. (1985). Seasonal distribution of chlorophyll-a in relation to physical structure in the western Irish Sea. *Oceanologica Acta*, **8(1)**, 77-86.
- Richardson, K., Visser, A. W., and Pedersen, F. B. (2000). Subsurface phytoplankton blooms fuel pelagic production in the North Sea. *Journal of Plankton Research*, **22(9)**, 1663-1671.
- Ridderinkhof, H. (1992). On the effects of variability in meteorological forcing on the vertical structure of a stratified water column. *Continental Shelf Research*, **12(1)**, 25-36.
- Rogachev, K. A., Carmack, E. C., Salomatin, A. S., and Alexanina, M. G. (2001). Lunar fortnightly modulation of tidal mixing near Kashevarov Bank, Sea of Okhotsk, and its impacts on biota and sea ice. *Progress in Oceanography*, **49(1-4)**, 373-390.
- Ross, O. N., and Sharples, J. (2004). Recipe for 1-D lagrangian particle-tracking models in space-varying diffusivity. *Limnology & Oceanography Methods*, **2**, 289-302.

- Ross, O. N., and Sharples, J. (2007). Phytoplankton motility and the competition for nutrients in the thermocline. *Marine Ecology Progress Series*, **347**, 21-38.
- Ruardij, P., van Haren, H., and Ridderinkhof, H. (1997). The impact of thermal stratification on phytoplankton and nutrient dynamics in shelf seas: a model study. *Journal of Sea Research*, **38(3-4)**, 311-331.
- Russell, R. W., Harrison, N. M., and Hunt, G. L. (1999). Foraging at a front: hydrography, zooplankton, and avian planktivory in the northern Bering Sea. *Marine Ecology-Progress Series*, **182**, 77-93.
- Sharples, J. (1999). Investigating the seasonal vertical structure of phytoplankton in shelf seas. *Progress in Oceanography*, **Suppl. S**, 3-38.
- Sharples, J. and Holligan, P. M. (2006). Interdisciplinary processes in the Celtic Seas. In: Robinson, A. R., and Brink, K. H. (eds.), *The Sea*, vol 14B, Harvard University Press, Cambridge MA, 1003-1031.
- Sharples, J., Moore, C. M., Rippeth, T. P., Holligan, P. M., Hydes, D. J., Fisher, N. R. and Simpson, J. H. (2001). Phytoplankton distribution and survival in the thermocline. *Limnology and Oceanography*, **46(3)**, 486-496.
- Sharples, J., Ross, O. N., Scott, B. E., Greenstreet, S. P. R., and Fraser, H. (2006). Inter-annual variability in the timing of stratification and the spring bloom in the North-western North Sea. *Continental Shelf Research*, **26(6)**, 733-751.
- Sharples, J. and Simpson, J. H. (1996). The influence of the springs-neaps cycle on the position of shelf sea fronts. In: Aubrey, D. G., and Friedrichs, C. T. (eds.), *Buoyancy effects on coastal and estuarine dynamics*, AGU, Washington D. C., 71-82.
- Sharples, J. and Tett, P. (1994). Modeling the effect of physical variability on the midwater chlorophyll maximum. *Journal of Marine Research*, **52(2)**, 219-238.
- Sharples, J., Tweddle, J. F., Green, J. A. M., Palmer, M. R., Kim, Y-N., Hickman, A. E., Holligan, P. M., Moore, C. M., Rippeth, T. P., Simpson, J. H., and Krivtsov, V. (2007). Spring-neap modulation of internal tide mixing and vertical nitrate fluxes at a shelf edge in summer. *Limnology and Oceanography*, **52(5)**, 1735-1747.
- Simpson, J. H. (1981). The shelf-sea fronts - implications of their existence and behavior. *Philosophical Transactions of the Royal Society of London*, **A302**, 531-546.
- Simpson, J. H. and Bowers, D. G. (1981). Models of stratification and frontal movement in shelf seas. *Deep Sea Res. A*, **27**, 727-738.
- Simpson, J. H. and Bowers, D. G. (1984). The role of tidal stirring in controlling the seasonal heat cycle in shelf seas. *Annales Geophysicae*, **2(4)**, 411-416.
- Simpson, J. H., Crawford, W. R., Rippeth, T. P., Campbell, A. R., and Cheok, J. V. S. (1996). The vertical structure of turbulent dissipation in shelf seas. *Journal of Physical Oceanography*, **26(8)**, 1579-1590.
- Simpson, J. H. and Hunter, J. R. (1974). Fronts in the Irish Sea. *Nature*, **250**, 404-406.
- Simpson, J. H., and Sharples, J. (1994). Does the earth's rotation influence the position of shelf sea fronts? *Journal of Geophysical Research*, **99(C2)**, 3315-3319.
- Sims, D. W. and Quayle, V. A. (1998). Selective foraging behaviour of basking sharks on zooplankton in a small-scale front. *Nature*, **393**, 460-464.
- Tett, P. B., Joint, I. R., Purdie, D. A., Baars, M., Oosterhuis, S., Daneri, G., Hannah, F., Mills, D. K., Plummer, D., Pomroy, A. J., Walne, A. W., and Witte, H. J. (1993). Biological consequences of tidal stirring gradients in the North Sea. *Philosophical Transactions of the Royal Society of London*, **A343**, 493-508.

- Trimmer, M., Gowen, R. J., Stewart, B. M., and Nedwell, D. B. (1999). The spring bloom and its impact on benthic mineralisation rates in western Irish Sea sediments. *Marine Ecology Progress Series*, **185**, 37-46.
- Waniek, J. J. (2003). The role of physical forcing in initiation of spring blooms in the northeast Atlantic. *Journal of Marine Systems*, **39(1-2)**, 57-82.
- Weston, K., Fernand, L., Mills, D. K., Delahunty, R., and Brown, J. (2005). Primary production in the deep chlorophyll maximum of the central North Sea. *Journal of Plankton Research*, **27(9)**, 909-922.
- Yin, K. D., Harrison, P. J., Pond, S., and Beamish, R. J. (1995). Entrainment of nitrate in the Fraser River Estuary and its biological implications, 3: effects of winds. *Estuarine Coastal and Shelf Science*, **40(5)**, 545-558